ACS APPLIED MATERIALS & INTERFACES
Research Article
www.acsami.org

High-Performance Fully Nanostructured Photodetector with Single-Crystalline CdS Nanotubes as Active Layer and Very Long Ag Nanowires as Transparent Electrodes

Qinwei An, Xianquan Meng,* and Pan Sun

Key Laboratory of Artificial Micro-and Nano-structures, Ministry of Education and School of Physics and Technology, and Center for Nanoscience and Nanotechnology School of Physics and Technology, Wuhan University, Wuhan, Hubei 430072, People's Republic of China

Supporting Information

ABSTRACT: Long and single-crystalline CdS nanotubes (NTs) have been prepared via a physical evaporation process. A metal–semiconductor–metal full-nanostructured photodetector with CdS NTs as active layer and Ag nanowires (NWs) of low resistivity and high transmissivity as electrodes has been fabricated and characterized. The CdS NTs-based photodetectors exhibit high performance, such as lowest dark currents (0.19 nA) and high photoresponse ratio ($I_{light}/I_{dark} \approx 4016$) (among CdS nanostructure network photodetectors and NTs netwok photodetectors reported so far) and very low operation voltages (0.5 V). The photoconduction mechanism, including the formation of a Schottky barrier at the interface of Ag NW and CdS NTs and the effect of oxygen adsorption process on the Schottky barrier has also been provided in detail based on the studies of CdS NTs photodetector in air and vacuum. Furthermore, CdS NTs photodetector exhibits an enhanced photosensitivity as compared with CdS NWs photodetector. The enhancement in performance is dependent on the larger surface area of NTs adsorbing more oxygen in air and the microcavity structure of NTs with higher light absorption efficiency and external quantum efficiency. It is believed that CdS NTs can potentially be useful in the designs of 1D CdS-based optoelectronic devices and solar cells.

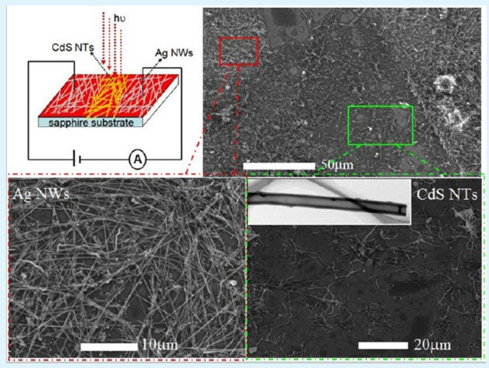

KEYWORDS: *photodetector, cadmium sulfide, nanotubes, nanowires, metal–semiconductor-metal structure*

INTRODUCTION

Photodetectors based on a large variety of semiconductor nanostructures have been widely studied, and considerable efforts have been devoted to developing a high-performance photodetector with a fast response time, good reproducibility, and high quantum efficiency. Due to large surface-to-volume ratios and Debye length comparable to their small sizes, one-dimensional (1D) inorganic nanostructures such as ZnO, ZnS, InSe, CdS, CdSe, ZnSe, Sb_2Se_3, AlN, ZrS_2, In_2Se_3, and Ag_2S nanowires/nanobelts/nanoparticles, have become the preferred materials to fabricate photodetector,[1−8] which have already displayed superior sensitivity to light and decent photodectoring property.

Among 1D inorganic nanostructures, cadmium sulfide (CdS), one of most studied II–VI semiconductors, exhibits a direct bandgap (~2.42 eV), relatively low work function, large refraction index, and excellent thermal and chemical stability, and has attracted more attention. Until now, the design and fabrication of CdS nanoscale photodetectors based on CdS nanowires,[9,10] nanobelts,[11,12] and nanorods[13] have been attempted. The aligned networks of CdS nanowires were used to fabricate photodetector and the photoconductive responses of the device were improved greatly due to the reduced conduction path between the electrodes and the decreased number of nanowire–nanowire junctions in the network, although the fabricated progress is complex.[9] Photodetector fabricated by CdS nanobelts displayed excellent properties resulted from surface trap states, short electrode distance, single crystalline character and large surface to volume ratio of the nanobelts.[11]

Recent research has also focused on exploring the effects of construction strategies for CdS nanoscale photodetectors on the performance of the devices. Photodetectors based on Schottky contact displayed unusually high sensitivities and short response time which mainly originates from the strong built-in electric fields, especially under reverse bias conditions.[10,14] Furthermore, metal semiconductor field effect transistor (MESFET) based single CdS nanobelt photodetector would efficiently lower the dark current at a gate voltage under light exposure and result in a fast response due to the strong electric field at the interface of the Schottky contact.[12] Through the progress of element doping,[15] composition, and bandgap

Received: July 9, 2015
Accepted: October 6, 2015
Published: October 6, 2015

DOI: 10.1021/acsami.5b06166
ACS Appl. Mater. Interfaces 2015, 7, 22941−22952

Table 1. Figures of Merit of CdS Nanostructure Photodetectors and Nanotube-based Photodetectors

photodetectors	dp	bias (V)	dark current (A)	photocurrent (A)	I_{photo}/I_{dark}	rise time	decay time	ref
CdS single nanobelt	width, 3 mm; thickness, 200 nm	0.5	6×10^{-6}	29×10^{-6}	4.8	20 ms	20 ms	11
CdS single nanobelt	thickness, 60 nm	5	37.2×10^{-12}	17.1×10^{-6}	4.6×10^{5}	76 ms	6 ms	30
CdS single nanobelt	width, 200 nm thickness,50 nm	5	2×10^{-11}	4×10^{-8}	2×10^{3}	1 s	1 s	31
CdS single nanowire	diam,200 nm	2.5	2×10^{-12}	2×10^{-7}	1×10^{5}	15 ms	15 ms	32
CdS single nanorod	diam,10~60 nm	1	1×10^{-9}	8.2×10^{-8}	82	170 ms	365 ms	11
CdS single nanowire	diam,158/243/481 nm	2	3×10^{-11}	2.4×10^{-10}	8	15 ms	15 ms	33
CdS single nanowire		−8	2×10^{-10}	3×10^{-8}	183		320 ms	10
CdS single nanobelt	width, 500 nm	−3.8	2.6×10^{-14}	7×10^{-8}	2.7×10^{6}	137 ms	379 ms	12
CdS nanowire aligned network		1	7×10^{-8}	1.4×10^{-7}	2	0.8 ms	240 ms	9
ZnO nanotubes network	diam,10 nm	1	9.53×10^{-9}	4.8×10^{-7}	50	150 s	250 s	19
TiO2 nanotubes + AAO network	diam, 100 nm	10	5×10^{-6}	3.5×10^{-5}	7	< 1s	< 1 s	20
TiO2 nanotubes network	diam, 100 nm	2.5	10^{-9}	2.5×10^{-4}	2.5×10^{5}	0.5 s	0.7 s	21
CdS nanotubes network	diam,200 ~ 300 nm	0.5	1.9×10^{-10}	7.63×10^{-7}	4016	0.82 s	0.63 s	this work
CdS nanowires network	diam, ~120 nm	0.5	2.92×10^{-9}	2.2×10^{-6}	741	0.4 s	0.7 s	

engineering,[16−18] an efficient way to tune the electrical transport properties and to reduce its bandgap of CdS nanostructures would lead to good stability, reproducibility, and fast response speed at zero bias voltage and enlarge its response range obviously. However, the doping and bandgap engineering technique must depend on the professional equipment. Therefore, it is still difficult to develop a high-performance photodetector that simultaneously meets the requirements of a fast response time, good reproducibility, and high quantum efficiency. This means that searching for new nanostructures with single crystalline character and large surface-to-volume ratio and exploring for new construction strategies with Schottky contact are necessary and urgent.

Nanotubes (NTs), owing to high surface-to-volume ratio, are beneficial for improving charge collection and charge carrier transportation, thus contributing to a higher photocurrent generation and enhancing performance of devices, but only ZnO nanotubes[19] and TiO_2 nanotubes[20,21] have been used to fabricate photodetectors. A photodetector based on ZnO nanotubes shows that the photocurrent (4.82×10^{-7} A) of NTs can be enhanced compared to that (0.571×10^{-7} A) of ZnO NWs. Additionally, it is demonstrated that the performance of CdS nanotubes was more advantageous than ZnO or TiO_2 in a solar device.[22] Apart from its large surface area contacted with an electrolyte as nanotubes, CdS NTs efficiently facilitate the hole transportation, decrease electron−hole recombination, and avoid electron loss during injection from semiconductor nanocrystals. In addition, CdS NTs form a direct and rapid transport channel for photogenerated electrons because the electron mobility in CdS material (210 cm^2 V^{-1} s^{-1}) is much higher than that in TiO_2 and ZnO. In 2014, we successfully grew single-crystal CdS NTs.[23] However, to the best of our knowledge, there is no report about CdS NTs-based photodetectors.

On the other hand, Ag NW-based transparent conductive films (TCFs) as electrodes provide a low-resistance electrical contact to the active layer of optoelectronic devices, have an excellent ability to transmit light, and are considered the most suitable substitute for indium tin oxide (ITO).[24,25] Therefore, AgNWs have been promising building blocks for fully integrated nanoscale photonic and optoelectronic devices.[26−29]

In this research, superlong single-crystalline CdS NTs were synthesized by vapor−liquid−solid (VLS) process. Then, an entirely novel type of high-sensitivity photodetector based on single-crystalline CdS NTs as active layer with AgNWs transparent film as electrodes was designed and fabricated. Characterization of the photodetector performance is pursued at very low operation voltages (0.5 V), resulting in the lowest dark currents (0.19 nA) and very high (4016) photo- to dark-current ratio among CdS nanostructure network photodetectors and ZnO NTs and TiO_2 NTs netwok photodetectors reported so far (Table 1). In particular, the device exhibited enhanced sensitivity (4016) and larger turn-on voltages (0.3 V) compared with the sensitivity (741) and turn-on (0.21 V) voltage of CdS nanowires photodetector with the same construction strategies. Furthermore, to elucidate the difference of photoconduction properties between NT-based devices and NW-based devices, we comparatively studied the photoconductivity of NT-based and NW-based devices in different ambient conditions (e.g., in air or under vacuum), and a physical model was developed to illustrate the origin of the photoconductive gain in semiconductor NTs where the high density of surface trap states and the microcavity structure of NTs suppress the dark current at the reverse bias modes and enhance light absorption efficiency and external quantum efficiency.

■ EXPERIMENTAL SECTION

Preparation of CdS Nanotubes and Ag Nanowires and Device Fabrication. Single-crystalline CdS NTs were synthesized using the thermal evaporation method as reported in our previous research (Supporting Information, part 1).[23] Very long Ag NWs were prepared by according to the successive microwave-assisted multistep growth (SMMG; Supporting Information, part 2).[29,34]

Ag NWs network with a transmittance and sheet resistance of 87% and 64Ω/sq, respectively, was used as the transparent electrodes of CdS NTs-based photodetectors. First, Ag NWs and CdS NTs were redispersed in ethanol, the ethanolic Ag NWs and CdS NTs can be dispersed simply by ultrasonic, thus being uniformly dispersed in the ethanol for further processing. Then, ethanolic Ag NWs were dispersed onto the sapphire substrates by spray coating using micro syringes. Following their deposition, transparent and conducting Ag NWs networks with uniform distribution and density were produced on the sapphire. To deposit CdS nanotubes between the drain and source Ag NWs electrodes, we provided a gap by mechanically

DOI: 10.1021/acsami.5b06166
ACS Appl. Mater. Interfaces 2015, 7, 22941−22952

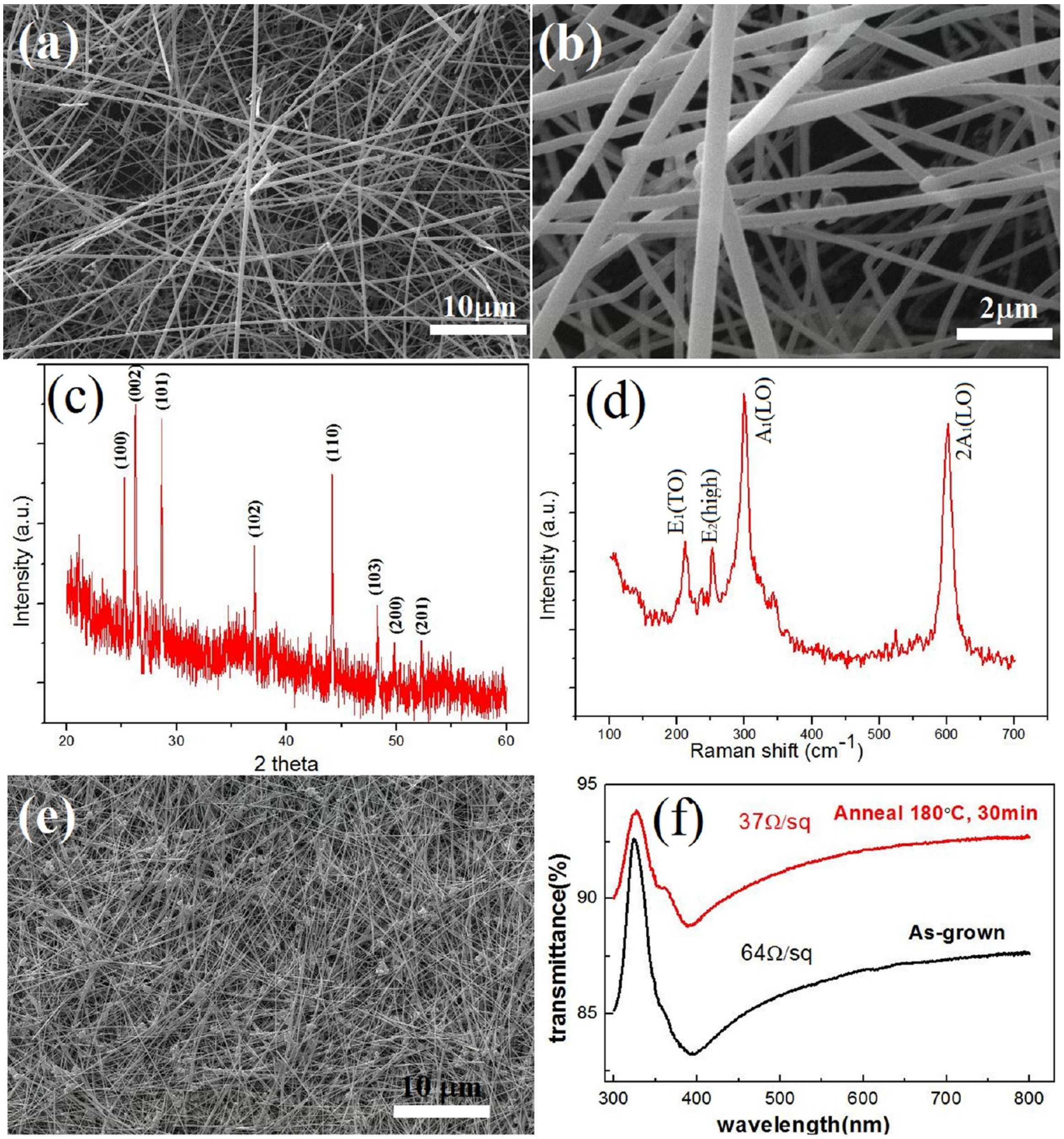

Figure 1. (a) Low-magnification and (b) high-magnification SEM images of CdS nanotubes. (c) XRD pattern and (d) Raman spectra of CdS nanotubes. (e) SEM image of Ag nanowires and (f) spectral transmittance and sheet resistance of synthesized AgNWs and after annealing 180 °C for 30 min.

scratching the substrate using a razor blade. A typical gap size between the drain and source Ag NWs electrodes was about 50 μm used for devices. Droplets containing large numbers of CdS NTs were placed the channel between the drain and source Ag NWs electrodes. CdS NT networks were fabricated between the drain and source Ag NWs electrodes through repeated spray coating and stamping process. To form a good contact and minimize the influence of contact resistance between Ag NW electrodes and CdS NTs, we carried out a fast annealing at 200 °C in Ar atmosphere for 5 min. At this stage, ultralong single-crystalline CdS-NTs based photodetectors have been fabricated to investigate its photoconducting properties.

Characterizations. The morphologies of the samples were observed by a JSM-6700 filed emission scanning electron microscope (FESEM). The crystalline structure of the samples was determined by X-ray diffraction (XRD) on Bruker-AXS D8 and transmission electron microscopy (TEM) on a JEM-2100 microscope (200 kV) with EDX attachment. Photoluminescence (PL) spectra were measured at room temperature using a He−Cd laser as excitation source (325 nm). Raman experiments were conducted at room temperature using a JY Horiba T64000 spectrometer equipped with cooled CCD detection and an Olympus BX40 confocal microscope with a 51× objective (spot size at the sample was ∼1 μm). Laser lines 532 nm (solid state green laser) at a flux of ∼180 $\mu W/\mu m^2$ was used as excitation sources.

Current−voltage ($I-V$) performance of the photodetector was measured by using Keithley 4200 system, and a xenon lamp (40 mW/cm^2) with around a 1.5 cm diameter circle illuminated area was used as the light source.

■ RESULTS AND DISSCUSSION

Figure 1a,b shows low- and high-magnification scanning electron microscopy (SEM) images of CdS nanotubes (NTs). The CdS nanotubes with a tangled morphology exhibit uniform density and size distribution, as shown in Figure 1a, and their lengths range from tens of micrometers to several hundreds of

DOI: 10.1021/acsami.5b06166
ACS Appl. Mater. Interfaces 2015, 7, 22941−22952

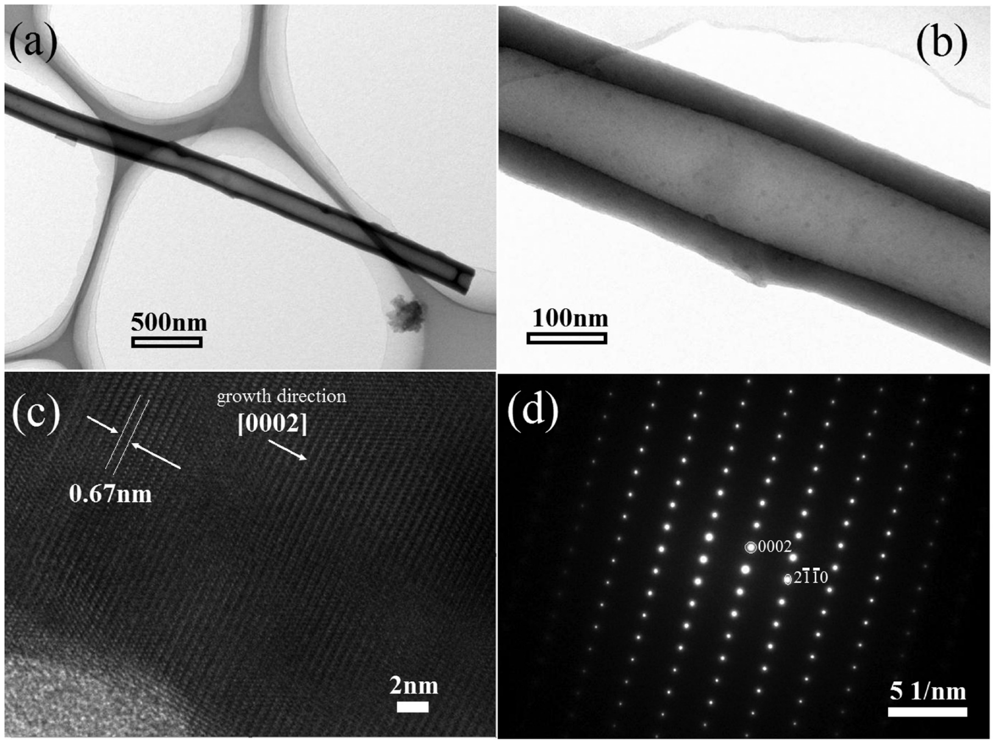

Figure 2. TEM and HRTEM analysis of CdS nanotubes. (a and b) TEM images of individual CdS nanotubes, corresponding to the (c) HRTEM image and (d) SAED pattern.

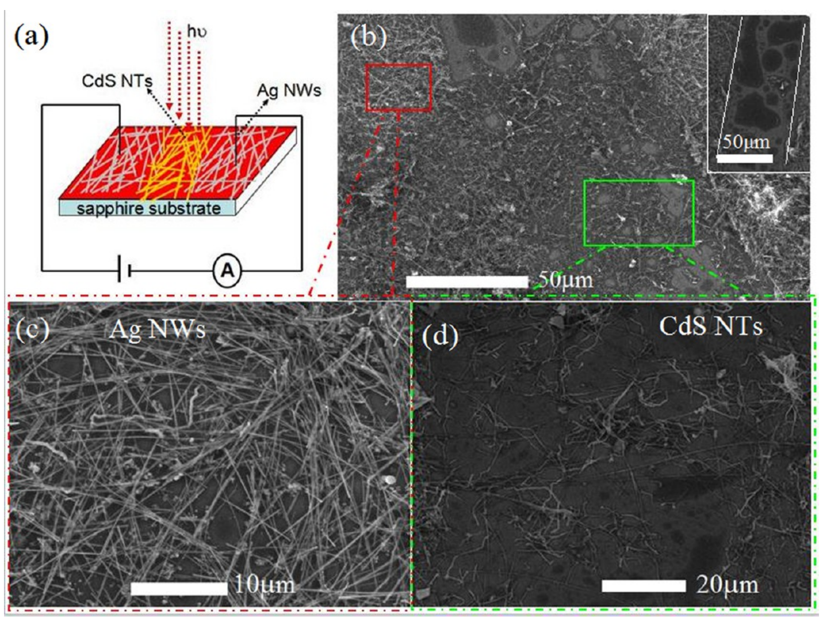

Figure 3. (a) Schematics of a CdS-nanotube fully nanostructured photodetector. (b) SEM image of the CdS-nanotube fully transparent photodetector. The inset shows that the channel was free from Ag NWs prior to CdS NTs transfer. Corresponding higher magnification SEM images of (c) Ag NWs network and (d) CdS nanotubes network.

micrometers. Figure 1b shows that the diameters of CdS nanotubes mostly range from 200 to 300 nm, and the diameter of an individual is uniform. The XRD pattern in Figure 1c is used to determine the crystal structure of CdS nanotbes, the peaks in the XRD pattern are identified according to The Inorganic Crystal Structure Database (ICSD) reference (PDF 00-041-1049). The diffraction peaks of (100), (002), (101), (102), (110), (103), (200), and (201) planes are labeled in the XRD pattern, which corresponds to the hexagonal wurtzite structure of CdS.

To further understand the structure of CdS nanotubes, we characterized the sample by Raman spectroscopy by analyzing the phonon active modes. The cadmium sulfide with the wurtzite crystal structure belongs to the space group $P6_3mc$ in international and C_{6V}^4 in Schönflies notation, and A_1, E_1, and E_2 symmetry modes are allowed for wurtzite CdS. The Raman active modes of E_1(TO), E_2(high), A_1(LO), and $2A_1$(LO)

DOI: 10.1021/acsami.5b06166
ACS Appl. Mater. Interfaces 2015, 7, 22941−22952

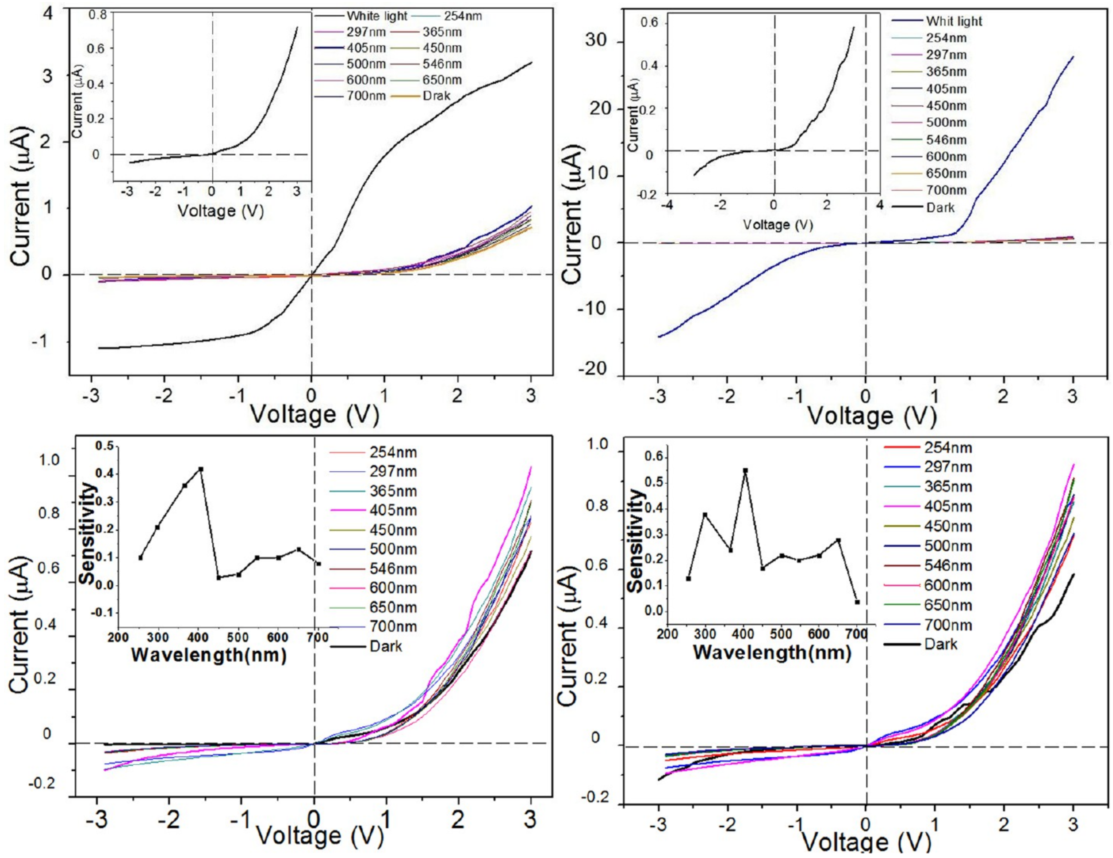

Figure 4. $I-V$ characteristics of the CdS-nanotube based fully nanostructured photodetector under xenon lamp illumination, different single wavelength light illumination and dark conditions (a) in air and (b) in vacuum, the corresponding inset shows the $I-V$ curves under dark condition. A series of tangents corresponding the different points of the $I-V$ curves with the voltage increasing are marked by Arabic numerals as shown in panels a and b. The magnified $I-V$ characteristics of the CdS nanotube based fully nanostructured photodetector under different single wavelength light illumination and dark conditions in (c) air atmosphere and (d) in vacuum. The corresponding inset shows the sensitivity as a function of the illumination of single-light wavelength at bias voltage of 2.0 V in air and in vacuum, respectively.

locates near 236.8, 252.6, 299.7, and 602.4 cm^{-1}, respectively, is clearly observed in Raman spectroscopy (Figure 1d),[35] proving that the structure of CdS nanotubes is wurtzite crystal structure. In addition, the Raman active mode was observed at 212.1 cm^{-1} is attributed to multiphonon response, similar multi-phonon response were observed in CdS nanobelts at 213 cm^{-1}[36] and in bulk CdS at 207 cm^{-1}.[35] Figure 1e displays the SEM image of Ag nanowires served as the transparent electrodes. The lengths of the Ag nanowires ranges from 50 to 70 μm and the diameters of Ag nanowires are around 100 nm. The transmittance spectra of as-grown AgNWs films spin-coated on a quartz glass and after annealing at 180 °C for 30 min are shown in Figure 1f. After annealing at 180 °C for 30 min, the long AgNW (red line) has larger transmittance than the as-grown AgNW (black line) over the tested wavelengths, and its sheet resistance reduced from 64Ω/sq to 38 Ω/sq after annealing due to fusing the overlapping nanowire junctions.[34]

The tubular structure and the crystal structure were also characterized by TEM and high-resolution TEM. TEM images of individual CdS nanotube shown in Figure 2a,b confirms the tubular structure of CdS nanotube and reveal that the outer diameter, inner diameter and wall thickness is about 211.4, 117.1, and 47.2 nm, respectively. The image of the high-resolution TEM in Figure 2c displays the lattice fringes of CdS nanotube with d spacing of 0.67 nm which corresponds to the interspace in the [0001] direction. Also the growth direction for CdS nanotube is determined to be [0001] which is indeed the thermodynamically favorable growth direction for wurtzite structures. The corresponding selected area diffraction (SAED) pattern (Figure 2d) indicates that CdS nanotubes are single crystals.

A schematic representation of the CdS-nanotube photo-detector is provided in Figure 3a. The corresponding SEM image of the device is shown in Figure 3b. A gap formed by mechanical scratching with a width of about 50 μm is free from Ag NWs (Figure 3b inset) and is then covered with CdS NTs by spin-coating progress. Figure 3c,d corresponds the magnified SEM image of rectangle A region and rectangle B region, as marked in Figure 3b, and clearly shows that Ag NWs network and CdS NTs network are about uniformly distributed on the substrate, respectively. Here, a semiconductor CdS NTs-Ag NWs junctions is formed in the network devices.

Figure 4a shows representative current−voltage ($I-V$) curves of the fabricated CdS-nanotube based photodetector under xenon lamp illumination, different single wavelength light illumination and dark conditions in air atmosphere as follows: dark, white light, and different single wavelength lights from 254 to 700 nm. A significant increase in the photocurrent of 622, 839, 1156, 1389, 4476, 79, 28, 14, 7, and 4 times is observed under bias voltages of −2.5, −2, −1.5, −1, −0.5, 0.5, 1, 1.5, 2, and 2.5 V, respectively. Figure 4b shows $I-V$ curves of the fabricated device under xenon lamp illumination, different single wavelength light illumination and dark conditions in vacuum as follow: dark, white light, and diffferent single wavelength lights from 254 to 700 nm. The increase in the photocurrent of 184, 281, 328, 345, 530, 26, 12, 29, 50, and 48 times is observed under bias voltages of −2.5, −2, −1.5, −1, −0.5, 0.5, 1, 1.5, 2, and 2.5 V, respectively. It is concluded that the increase ratios of photocurrent to dark current in air is striking larger than that in vacuum. The insets of Figure 4a,b show in detail the dark current of the fabricated CdS-nanotube based photodetector in air and in vacuum, respectively. It is observed that Schottky contacts form between CdS nanotubes and Ag nanowires due to *I*−*V* curves of photodetector showing the characteristics of diode rectifying. And the turn on-voltage of photodetector in air and in vacuum are about 0.3 and 0.1 V, respectively, obtained from the insets of Figure 4a,b.

In addition, by plotting tangents shown by the thin lines in Figure 4a,b, we can easily extrapolate the change trending of photo state conductivity value of CdS NTs in air atmosphere and in vacuum. With the increase of bias voltages, the photo state conductivity in vacuum throughout increase slowly, which is in agreement with the previous research,[9−11] while intriguingly, the photo state conductivity in air increase more largely and then increase slowly as indicated by the series of tangents marked by “1, 2, 3” in Figure 4a and “1, 2” in Figure 4b with the bias voltages increasing. Details will be discussed below.

The corresponding magnified *I*−*V* characteristic of the CdS-nanotube based fully nanostructured photodetector under different single wavelength light illumination and dark conditions in air atmosphere and in vacuum is shown in Figure 4c and Figure 4d, respectively. The insets of Figure 4c,d show sensitivity as a function of the illumination single light wavelength at bias voltage of 2.0 V in air and in vacuum, respectively. The sensitivity, typically calculated by the ratio between the amount of current change and the dark current $((I_{light} - I_{dark})/I_{dark})$.[1] The sensitivity of 0.42 in air and 0.55 in vacuum under the 405 nm single wavelength light illumination is more significant than that under other single-wavelength light illuminations, revealing the wavelength response of the CdS NT-based photodetector is highly selective whether in air or in vacuum.

Schematic diagram depicting the energy band in the CdS NTs-based photodetector are shown in Figure 5. Figure 5a,b show that because the work function of Ag (W_m = 4.26 V)[37] is lower than that of CdS (W_n = 4.2 V),[11] the conduction band (E_c) of CdS NTs upward bends due to the charge distribution during the formation of metal-semiconduction junction[37] and a Schottky contact forms[10] at the interface of Ag NW and CdS NTs.

Except the difference of intrinsic work function, the properties of material also have impact on the work function, for example the adsorbed oxygen molecules near the surface of CdS NTs.[38−41] The Fermi energy (E_F), depending on the properties of materials, is largely influenced by the change of conduction band (1 E_c) and valence band (E_v) and then affects the work function (W_n) of materials. In air atmosphere, the adsorbed oxygen molecules near the surface of CdS NTs would result in the formation of depletion layer and then lead to the further upward bending (ΔE_c) of the conduction and valence bands (ΔE_c)[3], as depicted in Figure 5c. Then, the Fermi energy shifts upward as the work function of CdS decreases. As a result, the energy barrier between Ag NWs and CdS NTs is increased in air atmosphere.

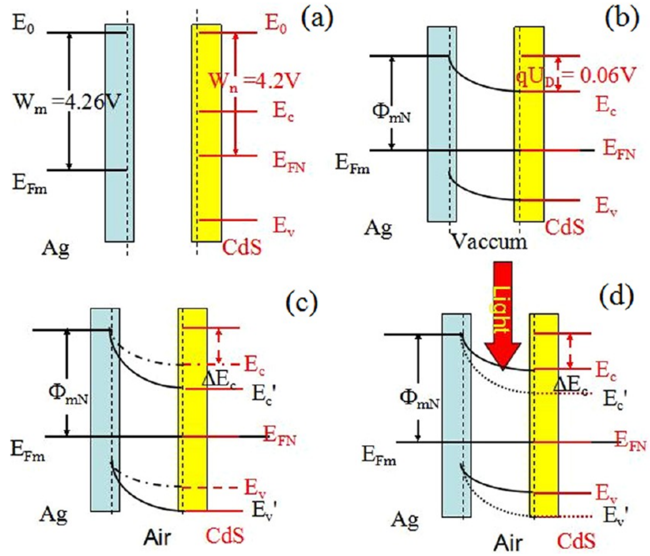

Figure 5. Energy band diagram for (a) separated CdS nanotube and Ag nanowires, (b) interconnected CdS nanotube and Ag nanowires, (c) interconnected CdS nanotube and Ag nanowires in air under dark condition, and (d) interconnected CdS nanotube and Ag nanowires in air under illumination condition.

The adsorbed oxygen molecules near the surface of CdS NTs leads to the larger Schottky barrier in air than that in vacuum. When operated at the reverse bias mode, the electrons would flow from Ag to CdS to overcome or tunnel through the Schottky barrier. The larger barrier in air results in that the rectification property to dark current is more obvious at the reverse bias mode as shown in the insets of Figure 4a,b. The good rectification property to dark current in air would lead to the striking increase of photocurrent and enhancement of the sensitivity in air for the NT-based photodetector.

For the NT-based photodetector, the energy barrier in vacuum is induced only by the difference of work function and its rectification properties is consistent with other researches.[9−11] However, the energy barrier in air is induced by both the difference of work function and the adsorbed oxygen molecules. When the device was illuminated by light with sufficient energy, electron−hole pairs are generated via the optical absorption and the photon-generated electron−hole pairs are then separated by the strong local electrical field existing at the Ag NW−CdS NW interface. Part of the adsorbed negatively charged oxygen ions combined with the holes and subsequently desorbed (which will be discussed later). Therefore, the barrier induced by adsorbed oxygen molecules vanishes as long as the device is subjected to illumination, as shown in Figure 5d. As a result, the photo state conductivity in air atmosphere increases largely and then increases slowly, and the forward bias increases as evaluated by the *I*−*V* curves slope and as indicated by the series of tangents (marked by “1, 2, 3” in Figure 4a and “1, 2” in Figure 4b) with the increasing bias voltages.

In a typical Schottky-contact-based devices (SCD), one of the two ohmic contact ends is replaced by a Schottky contact to build nonsymmetrical SCD.[10,42] And the *I*−*V* characteristics of SCD is asymmetric and a diodelike behavior is clearly observed.[10] Interestingly, the *I*−*V* characteristics of our CdS NT-based photodetector with a metal−semiconductor−metal configuration is asymmetric and a dilde-like rectifying behavior is observed. This result reveals that our CdS NT-based

DOI: 10.1021/acsami.5b06166
ACS Appl. Mater. Interfaces 2015, 7, 22941−22952

photodetector is not a simple symmetrical back-to-back Schottky contact and may be asymmetrical metal−semiconductor−metal network contacts with different numbers of CdS NT−Ag NW junction in the two contacts ends, as shown in Figure 3b, and different numbers of forward and reverse CdS NT−CdS NT junction barrier in the opposite direction of CdS NT network. Similarly, in ref 43, owing to different numbers of Zn_2GeO_4 NW-Zn_2GeO_4 NW junction, the two back-to-back Schottky barriers dominated by the NW-NW junction barriers was different and resulted in the asymmetric $I-V$ characteristics. Moreover, for the device with a metal−semiconductor−metal configuration and both contacts on CdS and Al, different numbers of CdS NW−CdS NW junction and CdS NW−Al electrode junction resulted in that the Schottky barrier of the two back-to-back Schottky contacts is different and $I-V$ nature in forward and reverse bias voltages is asymmetric in ref 44.

Here, we focus on the comparative studies of the work mechanism of NT-based photodetetor in air atmosphere with that in vacuum, as schematically presented in Figure 6. In the dark condition, the air atmosphere provides numerous oxygen molecules and the oxygen molecules adsorbed on the outer and inner surfaces of CdS NTs capture free electrons then depletion layer forms near outer and inner surfaces of CdS NTs as shown in Figure 6a. However, in vacuum condition, the oxygen molecules do not exist and thus the surface properties of CdS NTs are not changed. Under the illumination of xenon lamp, the energy of photons with wavelength smaller than 510 nm is larger than the bandgap of CdS (2.42 eV). Electron and hole pairs are generated on the surface of CdS NTs. As shown in Figure 6b, the photogenerated holes migrate to negatively charged oxygen ions and neutralize them. These neutralized oxygen molecules desorb from the outer and inner surfaces of CdS NTs. Finally, the adsorbed process and desorbed process of oxygen molecules reach a certain equilibrium. The electron and hole pairs are also generated on the surface of CdS NTs under illumination in vacuum, while the number of electron and hole is equal. Under an electric field, the electron and hole move in opposite directions at different velocities. Compared with the behavior in air, the current at forward bias in vacuum is larger than that in air atmosphere because the current in vacuum depends on both electrons and holes, while the current in air atmosphere only is dependent on the electrons, as shown in Figure 6c. It is natural that the photocurrent in vacuum is larger than that in air, as shown in the $I-V$ curves of Figure 4a,b.

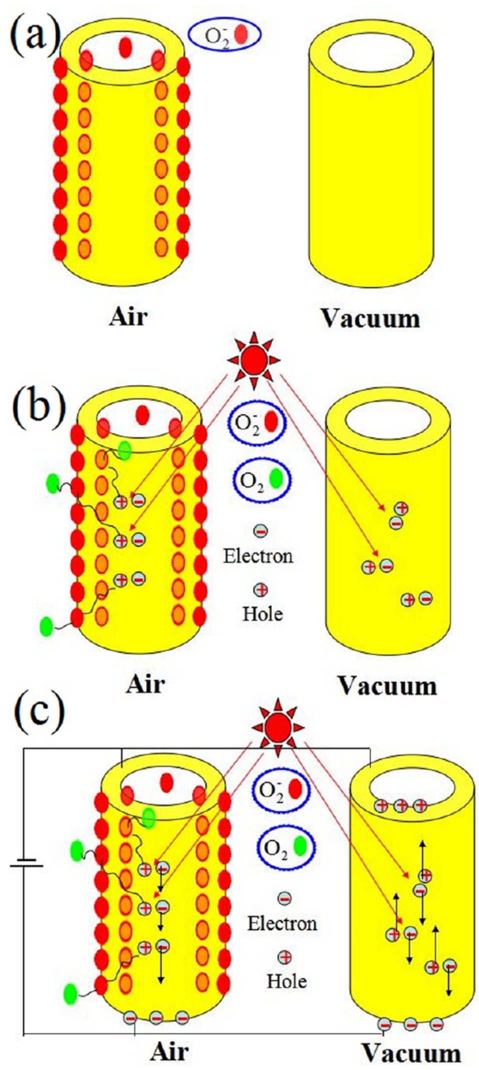

Figure 6. Schematic of the photoresponse process of CdS nanotube in air and in vacuum under (a) dark condition, (b) illumination condition, and (c) illumination condition with a bias voltage.

As an important evaluating index reflecting the capability of a photodetector to follow a fast-varying optical signal, the response speed is determined by the time response. The time responses of the CdS NTs based photodetector in air atmosphere and in vacuum are shown in Figure 7a,b, which are measured by periodic turning on the light at the reverse bias mode of 1 V. The CdS NTs based photodetector is highly stable and excellently reproducible.

The rise time (τ_{rise}) and fall time (τ_{fall}) are defined by measuring the time for the current increase from 10 to 90% of the saturation current and the current decrease from 90 to 10% of its saturation value, respectively. The rise time and fall time of the device in air atmosphere are 0.63 s and 0.8 s, respectively, which are in line with that for some single CdS nanostructure photodetectors and even smaller than that for nanotubes photodetectors (Table 1). The fall time is relatively larger than the rise time, which could be related to the deep trap level resulted from the defect on the CdS NTs surface.[5] Compared with that in air atmosphere, the rise time and fall time in vacuum at the same bias decrease to 0.22 and 0.15 s, respectively. However, the fall time is relatively lower compared with the rise time. The sensitivity of the photodetector is found to be 1881 in air and 352 in vacuum as determined from Figure 7a,b.

In addition, Figure 7c,d show the time response of photodetector in air and in vacuum at the forward bias of 1.5 V. Compared with that at reverse bias, the stability and reproducibility of present photodetector at forward bias mode is reduced clearly shown in Figures 7b and 5d. The sensitivities at reverse bias modes decrease to 10 in air and 19 in vacuum, and the rise time and fall time change to be 0.37 and 0.38 in air and 20.55 and 24.37 in vacuum, respectively. The critical parameters of CdS-NT-based photodetector are found to be different between air atmosphere and vacuum with increasing bias voltages, as summarized in Table 2.

Figure 7e,f depicts the sensitivity spectra of the CdS NTs-based photodetector as a function of the incident light wavelength at reverse bias of −0.5, −1, and −1.5 V in air and in vacuum, respectively. In air the sensitivity at reverse bias of

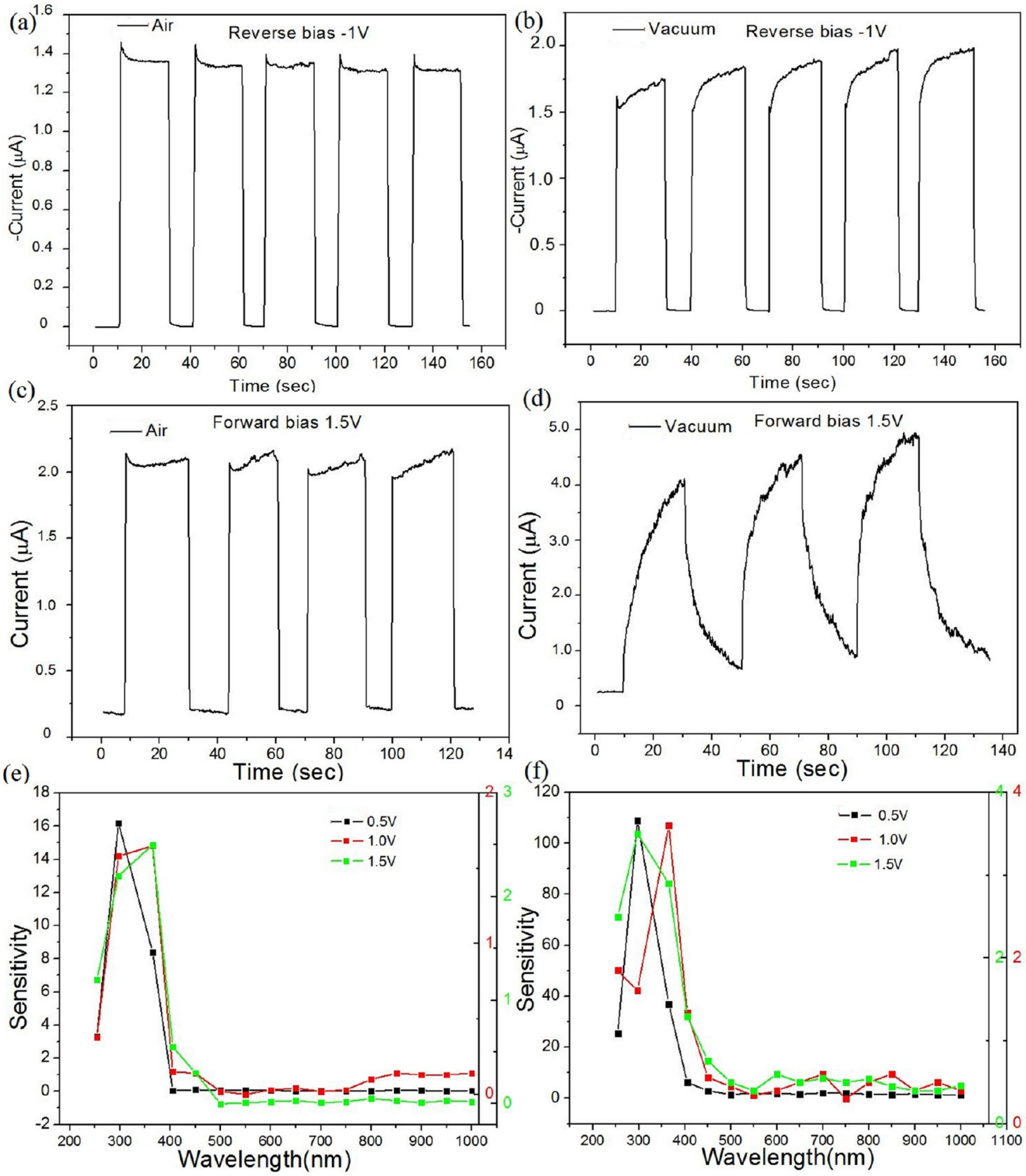

Figure 7. Response and recovery characteristics of the CdS-nanotube-based fully nanostructured photodetector with the light on/off switching in air atmosphere under the bias voltages of −1 (a) and (c) 1.5 V and in vacuum under the bias voltages of (b) −1 and (d) 1.5 V. The sensitivity spectra of the CdS-NTs-based photodetector as a function of the incident light wavelength at reverse bias of −0.5, −1, and −1.5 V in (e) in air and (f) in vacuum.

−1 V is more significant than that at reverse bias of −0.5 and −1.5 V. However, in vacuum, the sensitivity at reverse bias of −0.5 V is more significant than that at reverse bias of −1 and −1.5 V. At three different reverse biases, a peak sensitivity from 297 to 365 nm with a narrow band is achieved whether in air atmosphere or in vacuum, revealing that the responsivity of the CdS NTs-based photodetector is highly selective and revealing the high stability and repeatability of the device.

To further understand the mechanism and explore the potential merits of the CdS-NT-based photodetector, we have also fabricated the corresponding CdS NWs-based photodetector to investigate them comparatively. Figure 8a shows the SEM image of CdS nanowires synthesized at 850 °C for 60 min by the thermal evaporation of CdS powder. The CdS nanowires with a tangled morphology have diameters around ∼120 nm and lengths up to a few tens of micrometers. High diameter uniformity over the whole length of CdS nanowires is noted from the low-magnification TEM images in Figure 8b. The corresponding high-resolution TEM image and SAED pattern shown in Figure 8c,d demonstrate that the CdS nanowires with wurtzite structures is single-crystalline.

It is interesting to study the advantage for the CdS-NT-based photodetector compared with CdS NW-based photodector. Figure 9a,b shows the $I-V$ curves of CdS NW-based photodector in air atmosphere and in vacuum, respectively, under dark and white light illumination conditions. Both $I-V$

Table 2. Comparison of Critical Parameters of the CdS-NT-based Photodetector with Increasing Bias Voltages in Air Atmosphere and in Vacuum

bias (V)	I (light)	I (dark)	sensitivity	photoresponse (s) rise time	photoresponse (s) fall time
Air Atmosphere					
−0.5	7.63×10^{-7}	1.9×10^{-10}	4016	0.82	0.63
−1	1.36×10^{-6}	7.23×10^{-10}	1881	0.63	0.8
−1.5	1.65×10^{-6}	1.22×10^{-9}	1352	0.71	0.46
−2	2.27×10^{-6}	2.32×10^{-9}	978	0.8	0.48
1	1.92×10^{-6}	9.83×10^{-8}	20	0.37	0.31
1.5	2.06×10^{-6}	2.0×10^{-7}	10	0.37	0.38
Vacuum					
−0.5	4.56×10^{-7}	8.49×10^{-10}	537	0.64	0.43
−1	1.92×10^{-6}	5.44×10^{-9}	353	0.22	0.15
−1.5	4.62×10^{-6}	1.42×10^{-8}	325	0.38	5.38
−2	8.22×10^{-6}	2.97×10^{-8}	277	0.6	5.92
1	2×10^{-6}	1.99×10^{-7}	10	7.06	20.06
1.5	4.91×10^{-6}	2.63×10^{-7}	19	20.55	24.37

curves under dark condition in air atmosphere and in vacuum show Schottky contact characteristics, and the intensities of the dark current at the same bias modes in air are smaller than that in vacuum, indicating that oxygen adsorption is indeed facilitated to trap electrons and increase the height of barriers.

Furthermore, the turn on voltage of photodetector in air and in vacuum are about 0.21 and 0.04 V, respectively. We can see the turn-on voltage (V_T) shifts from 0.3 to 0.21 V in air and from 0.1 to 0.04 V in vacuum when CdS NTs as active layer is replaced by CdS NWs, directly indicating that NTs facilitate the oxygen adsorption and increase largely the height of barrier.

Besides, compared with the photocurrent in air, the photocurrent in vacuum is significantly enhanced. And the difference of the photo state conductivity between in air and in vacuum evaluated by plotting I as a function of V, which can be explained by the similar analysis for the NT-based photodector. However, nearly symmetrical photocurrent behavior in air atmosphere and in vacuum are observed, implying the difference of Schottky barrier for the two back-to-back Schottky contacts in the NW-based device is smaller than that in the NT-based device.

Figure 9c,d shows the time response of CdS NWs-based photodetector under bias of −1 and 1 V in air atmosphere. The present photodetector in air atmosphere is highly stable and reproducible. The sensitivity of the device is 694 and 647, and the corresponding rise time and fall time are 0.3 and 0.7s and 0.4 and 0.7s under the reverse bias of −1 V and under the forward bias of 1 V, respectively. Due to the smaller dark current under the reverse bias of −1 V, the sensitivity in air under reverse bias mode is slightly enhanced.

Compared with the performance of the NW-based photodetector under the reverse bias mode, the sensitivity for the NT-based photodetector is significantly larger than that for the NW-based device, which could be due to the larger surface area of CdS NTs where more oxygen molecules adsorbed on the surface of CdS NTs and would capture more free electrons. The height and width of the barrier induced by formed depletion layer near the NTs surface is larger than those on the surface of NWs. Besides, according to the detailed discussion about the mechanism of the CdS NTs-based photodetector, it is well-known that the dark current in vacuum is only dependent on the Schottky contact at the interface of Ag NW and CdS NTs induced by the difference of intrinsic work

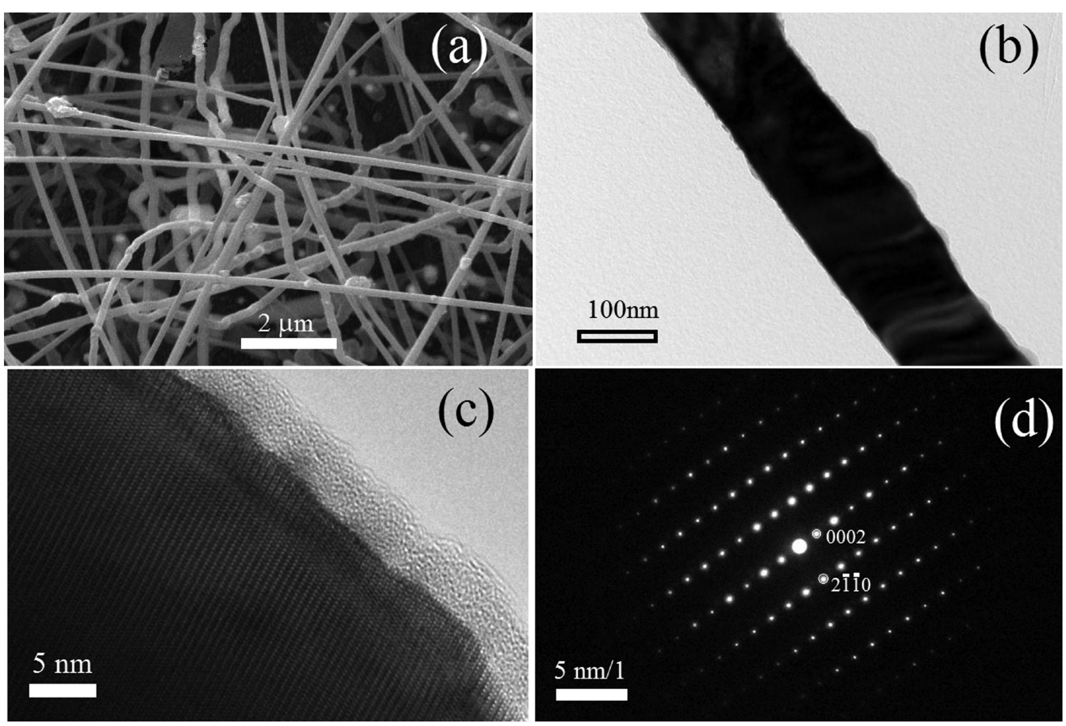

Figure 8. SEM, TEM, and HRTEM analyses of CdS nanowires. (a) SEM and (b) TEM images of CdS nanowires and corresponding (c) HRTEM image and (d) SAED pattern.

DOI: 10.1021/acsami.5b06166
ACS Appl. Mater. Interfaces 2015, 7, 22941−22952

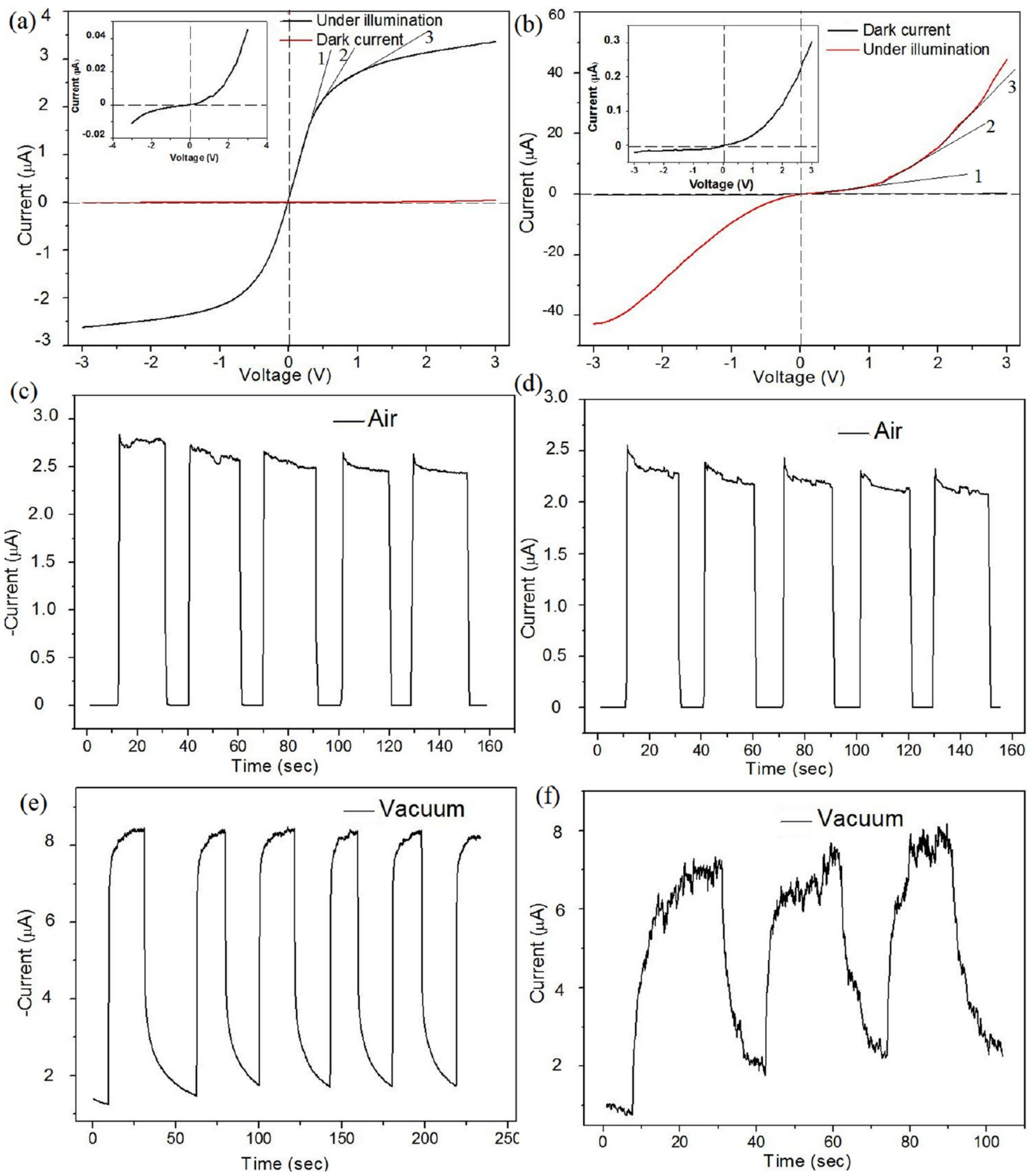

Figure 9. *I*−*V* characteristics of the CdS-nanowire based fully nanostructured photodetector under white light illumination and dark conditions in (a) air atmosphere and (b) vacuum atmosphere. Response and recovery characteristics of the CdS-nanowire-based fully transparent photodetector with the light on/off switching in air atmosphere with bias (c) −1 and (d) 1 V and in vacuum with bias (e) −1 and (f) 1 V.

function. Except the difference of intrinsic work function, the dark current in air is related to the adsorbed oxygen molecules near the surface of CdS NTs. It is concluded that CdS NTs-based device with large surface area has a significant Schottky barrier improvement than CdS NWs-based device.

In addition, CdS NTs, having a hollow structure where the shell and hollow area have different indexes of refraction, can be considered as a natural microcavity. It is demonstrated that microcavity structures can control spontaneous emission[45] and improve external quantum efficiency[46] and the color purity[47] and thus has been applied in organic electroluminescent devices[45] and organic light-emitting devices (OLEDs).[46] Therefore, the microcavity structure of NTs may be helpful for light absorption of photodetecter and favorable for generating more electron−hole pairs due to the higher external quantum efficiency.

Additionally, it had been demonstrated that the performance of CdS NTs is more advantageous in solar devices[22] due to its large surface area contacted with an electrolyte, which efficiently facilitates hole transportation, decreases electron−hole recombination, and forms a direct and rapid transport channel for photogenerated electrons. Consequently, the performance enhancement of NT-based devices also may benefit from the improvement of the electron and hole flow modulation ability both in Schottky barrier characteristics (1 SBH and SBW) and electron and hole flow channel. These advantages of NTs-based device provide us a chance to develop

DOI: 10.1021/acsami.5b06166
ACS Appl. Mater. Interfaces 2015, 7, 22941−22952

a high-performance photodetector with a fast response time and good reproducibility.

The time response of the device under bias of −1 and 1 V in vacuum are shown in Figure 9e,f. The stability and reproduciblility of the NW-based photodecetor dramatically decrease. The sensitivity of the device is 5.5 and 2.0, and the corresponding rise time and fall time are 8.2s and 9.8s and 6.7s and 6.4s under the reverse bias of −1 V and under the forward bias of 1 V, respectively. Because of nonoxygen-absorbing in vacuum, the NW-based device lacks the electron and hole flow modulation ability both in electron flow channel and Schottky barrier characteristics (1 SBH and SBW) through oxygen adsorption−desorption, as discussed in air atmosphere. The lower sensitivity of the device comes from the increasing charge carrier density resulted from the strong local electrical field existing at the NW-Ag interface. And because the photogenerated holes need not migrate to negatively charged oxygen ions and neutralize them, the resulting current in vacuum is much larger than that in air, which is in good agree with the scales of the vertical axis of $I-V$ curves, shown in Figure 9a,b. These values under other bias modes of NW-based device are summarized in Table 3.

Table 3. Comparison of Critical Parameters of CdS NW-based Photodetector with Increasing Bias Voltages in Air Atmosphere and in Vacuum

Air Atmosphere					
				photoresponse (s)	
bias (V)	I (light)	I (dark)	sensitivity	rise time	fall time
−2.5	-3.27×10^{-6}	-7.55×10^{-9}	433	0.4	0.6
−2	-3.27×10^{-6}	-6.03×10^{-9}	542	0.9	0.6
−1.5	-3.5×10^{-6}	-5.54×10^{-9}	632	0.4	0.3
−1	-2.5×10^{-6}	-3.6×10^{-9}	694	0.3	0.7
−0.5	-1.57×10^{-6}	-3.12×10^{-9}	503	0.5	0.7
0.5	2.2×10^{-6}	2.97×10^{-9}	741	0.4	0.7
1	2.2×10^{-6}	3.4×10^{-9}	647	0.4	0.7
1.5	2.5×10^{-6}	7.9×10^{-9}	316	0.8	0.7
2	3.69×10^{-6}	1.51×10^{-8}	244	0.5	1
2.5	8.3×10^{-6}	4.5×10^{-8}	184	0.4	7.9
Vacuum					
				photoresponse (s)	
bias (V)	I (light)	I (dark)	sensitivity	rise time	fall time
−2.5	-6.7×10^{-5}	-5.76×10^{-6}	1.1	8.8	10.5
−2	-3.7×10^{-5}	-5.4×10^{-6}	6.9	3.2	6.3
−1.5	-1.8×10^{-5}	-3.3×10^{-6}	5.5	2.3	9.6
−1	-8.2×10^{-6}	-1.5×10^{-6}	5.5	8.2	9.8
−0.5	-7×10^{-6}	-2.2×10^{-6}	3.2	5.1	6.7
0.5	1.23×10^{-6}	3.7×10^{-7}	3.3	7.4	11.9
1	3.7×10^{-6}	1.9×10^{-6}	2.0	6.7	6.4
2	3.5×10^{-5}	4.1×10^{-6}	8.5	9.2	10.5

CONCLUSION

In summary, long and single-crystalline CdS nanotubes have been prepared via a physical evaporation process. CdS NTs are first used to assemble the active layer of photodetectors with AgNWs transparent network of low resistivity and high transmissivity as electrodes. The CdS NTs photodetector features very low operation voltages (0.5 V), lowest dark currents (0.19 nA), and the very high (4016) photo to dark current ratio among CdS nanostructure network photodetectors and ZnO NTs and TiO_2 NTs netwok photodetectors reported so far. This excellent performance was attributed to the formation of Schottky barrier at the interface between Ag NW and CdS NTs and the effect of oxygen adsorption process on the Schottky barrier by investigation of CdS NTs photodetector in air or vacuum. Adsorbing oxygen molecules on the surface of CdS NTs and then capturing more free electrons increase the height and width of the Schottky barrier and decrease the conductance of NTs. Therefore, the dark current of photodetector is suppressed at the reverse bias modes, and the sensitivity is enhanced.

Furthermore, CdS NTs photodetector exhibits an enhanced photoresponse as compared with CdS NWs photodetector. The enhanced performance is dependent on the larger surface area of NTs with more oxygen-adsorbed states that have the advantages of greatly reducing the dark current and the microcavity structure of NTs which may be helpful for light absorption of photodetecter and favorable for generating more electron−hole pairs due to the improved external quantum efficiency. CdS NTs with remarkable application potential opens a way for developing higher sensitivity, higer external quantum efficiency and powder-saving photodectors or sensors.

ASSOCIATED CONTENT

Supporting Information

The Supporting Information is available free of charge on the ACS Publications website at DOI: 10.1021/acsami.5b06166.

The detailed experimental process for fabrication of superlong CdS nanotubes and synthesis of very long Ag nanowire. (PDF)

AUTHOR INFORMATION

Corresponding Author

*E-mail: mengxq3413@hotmail.com.

Notes

The authors declare no competing financial interest.

ACKNOWLEDGMENTS

This work was financially supported by the National Natural Science Foundation of China under Grant (No. 11275144 and No. J1210061).

REFERENCES

(1) Deng, K. M.; Li, L. CdS Nanoscale Photodetectors. *Adv. Mater.* **2014**, *26*, 2619−2635.

(2) Zheng, W.; Huang, F.; Zheng, R. S.; Wu, H. L. Low-Dimensional Structure Vacuum-Ultraviolet-Sensitive (λ< 200 nm) Photodetector with Fast-Response Speed Based on High-Quality AlN Micro/Nanowire. *Adv. Mater.* **2015**, *27*, 3921.

(3) Afal, A.; Coskun, S.; Emrah Unalan, H. All Solution Processed, Nanowire Enhanced Ultraviolet Photodetectors. *Appl. Phys. Lett.* **2013**, *102*, 043503−043508.

(4) Yan, C. Y.; Wang, J. X.; Wang, X.; Kang, W. B.; Cui, M. Q.; Foo, C. Y.; Lee, P. S. An Intrinsically Stretchable Nanowire Photodetector with a Fully Embedded Structure. *Adv. Mater.* **2014**, *26*, 943−950.

(5) Mulazimoglu, E.; Coskun, S.; Gunoven, M.; Butun, B.; Ozbay, E.; Turan, R.; Unalan, H. E. Silicon Nanowire Network Metal-Semiconductor-Metal Photodetectors. *Appl. Phys. Lett.* **2013**, *103*, 083114−083119.

(6) Nasiri, N. S.; Bo, R. H.; Wang, F.; Fu, L.; Tricoli, A. Ultraporous Electron-Depleted ZnO Nanoparticle Networks for Highly Sensitive Portable Visible-Blind UV Photodetectors. *Adv. Mater.* **2015**, *27*, 4336.

(7) Zhai, T. Y.; Li, L.; Wang, X.; Fang, X. S.; Bando, Y.; Golberg, D. Recent Developments in One-Dimensional Inorganic Nanostructures for Photodetectors. *Adv. Funct. Mater.* **2010**, *20*, 4233−4248.
(8) Fang, X. S.; Wu, L. M.; Hu, L. F. ZnS Nanostructure Arrays: A Developing Material Star. *Adv. Mater.* **2011**, *23*, 585−598.
(9) Heo, K.; Lee, H.; Park, Y.; Park, J.; Lim, H. J.; Yoon, D.; Lee, C.; Kim, M.; Cheong, H.; Park, J.; Jian, J.; Hong, S. Aligned Networks of Cadmium Sulfide Nanowires for Highly Flexible Photodetectors with Improved Photoconductive Responses. *J. Mater. Chem.* **2012**, *22*, 2173−2179.
(10) Wei, T. Y.; Huang, C. T.; Hansen, B. J.; Lin, Y. F.; Chen, L. J.; Lu, S. Y.; Wang, Z. L. Large Enhancement in Photon Detection Sensitivity via Schottky-gated CdS Nanowire Nanosensors. *Appl. Phys. Lett.* **2010**, *96*, 013508−013511.
(11) Li, L.; Wu, P. C.; Fang, X. S.; Zhai, T. Y.; Dai, L.; Liao, M. Y.; Koide, Y.; Wang, H. Q.; Bando, Y.; Golberg, D. Single-Crystalline CdS Nanobelts for Excellent Field-Emitters and Ultrahigh Quantum-Effi ciency Photodetectors. *Adv. Mater.* **2010**, *22*, 3161−3165.
(12) Ye, Y.; Dai, L.; Wen, X. N.; Wu, P. C.; Pen, R. M.; Qin, G. G. High-Performance Single CdS Nanobelt Metal-Semiconductor Field-Effect Transistor-Based Photodetectors. *ACS Appl. Mater. Interfaces* **2010**, *2*, 2724−2727.
(13) Jie, J. S.; Zhang, W. J.; Jiang, Y.; Meng, X. M.; Li, Y. Q.; Lee, S. T. Photoconductive Characteristics of Single-Crystal CdS Nanoribbons. *Nano Lett.* **2006**, *6*, 1887−1892.
(14) Dufaux, T.; Burghard, M.; Kern, K. Efficient Charge Extraction out of Nanoscale Schottky Contacts to CdS Nanowires. *Nano Lett.* **2012**, *12*, 2705−2709.
(15) Wu, C. Y.; Jie, J. S.; Wang, L.; Yu, Y. Q.; Peng, Q.; Zhang, X. W.; Cai, J. J.; Guo, H.; Wu, D.; Jiang, Y. Chlorine-doped n-type CdS Nanowires with Enhanced Photoconductivity. *Nanotechnology* **2010**, *21*, 505203−505210.
(16) Choi, Y. J.; Park, K. S.; Park, J. G. Network-bridge Structure of CdS_xSe_{1-x} Nanowire-based Optical Sensors. *Nanotechnology* **2010**, *21*, 505605−505610.
(17) Takahashi, T.; Nichols, P.; Takei, K.; Ford, A.; Jamshidi, A.; Wu, M. C.; Ning, C. Z.; Javey, A. Contact Printing of Compositionally Graded CdSxSe1-x Nanowire Parallel Arrays for Tunable Photodetectors. *Nanotechnology* **2012**, *23*, 045201−045205.
(18) Li, L.; Lu, H.; Yang, Z. Y.; Tong, L. M.; Bando, Y.; Golberg, D. Bandgap-Graded CdS_x Se_{1-x} Nanowires for High-Performance Field-Effect Transistors and Solar Cells. *Adv. Mater.* **2013**, *25*, 1109−1113.
(19) Chantarat, N.; Chen, Y. W.; Chen, S. Y.; Lin, C. C. Enhanced UV Photoresponse in Nitrogen Plasma ZnO Nanotubes. *Nanotechnology* **2009**, *20*, 95201−95206.
(20) Chang, Y. H.; Liu, C. M.; Tseng, Y. C.; Chen, C.; Chen, C. C.; Cheng, H. E. Direct Probe of Heterojunction Effects upon Photoconductive Properties of TiO_2 Nanotubes Fabricated by Atomic Layer Deposition. *Nanotechnology* **2010**, *21*, 225602−225609.
(21) Zou, J. P.; Zhang, Q.; Huang, K.; Marzari, N. Ultraviolet Photodetectors Based on Anodic TiO2 Nanotube Arrays. *J. Phys. Chem. C* **2010**, *114*, 10725−10729.
(22) Ling, T.; Wu, M. K.; Du, X. W. Template Synthesis and Photovoltaic Application of CdS Nanotube Arrays. *Semicond. Sci. Technol.* **2012**, *27*, 055017−055024.
(23) An, Q. W.; Meng, X. Q.; Zhang, L.; Zhao, Y. J. Controllable Growth of Single Crystalline CdS Nanotubes by Thermal Evaporation. *Mater. Lett.* **2014**, *136*, 55−58.
(24) Peng, S. M.; Su, Y. K.; Ji, L. W.; Young, S. J.; Tsai, C. N.; Hong, J. H.; Chen, Z. S.; Wu, C. Z. Transparent ZnO Nanowire-Network Ultraviolet Photosensor. *IEEE Trans. Electron Devices* **2011**, *58*, 2036−2040.
(25) De, S.; Higgins, T.; Lyons, P.; Doherty, E.; Nirmalraj, P.; Blau, W.; Boland, J.; Coleman, J. Silver Nanowire Networks as Flexible, Transparent, Conducting Films: Extremely High DC to Optical Conductivity Ratios. *ACS Nano* **2009**, *3*, 1767−1774.
(26) Yu, Z. B.; Li, L.; Zhang, Q. W.; Hu, W. L.; Pei, Q. B. Silver Nanowire-Polymer Composite Electrodes for Efficient Polymer Solar Cells. *Adv. Mater.* **2011**, *23*, 4453−4457.
(27) Morgenstern, F. S. F.; Kabra, D.; Massip, S.; Brenner, T. J. K.; Lyons, P. E.; Coleman, J. N.; Friend, R. H. Ag-nanowire Films Coated with ZnO Nanoparticles as a Transparent Electrode for Solar Cells. *Appl. Phys. Lett.* **2011**, *99*, 183307−183310.
(28) Rossouw, D.; Couillard, M.; Vickery, J.; Kumacheva, E.; Botton, G. A. Multipolar Plasmonic Resonances in Silver Nanowire Antennas Imaged with a Subnanometer Electron Probe. *Nano Lett.* **2011**, *11*, 1499−1504.
(29) Lee, J.; Lee, P.; Lee, H.; Lee, D.; Lee, S. S.; Ko, S. H. Very long Ag Nanowire Synthesis and Its Application in a Highly Transparent, Conductive and Flexible Metal Electrode Touch Panel. *Nanoscale* **2012**, *4*, 6408−6414.
(30) Li, Q. H.; Gao, T.; Wang, T. H. Optoelectronic Characteristics of Single CdS Nanobelts. *Appl. Phys. Lett.* **2005**, *86*, 193109−193011.
(31) Gao, T.; Li, Q. H.; Wang, T. H. CdS Nanobelts as Photoconductors. *Appl. Phys. Lett.* **2005**, *86*, 173105−173107.
(32) Gu, Y.; Kwak, E. S.; Lensch, J. L.; Allen, J. E.; Odom, T. W.; Lauhon, L. J. Near-field Scanning Photocurrent Microscopy of a Nanowire Photodetector. *Appl. Phys. Lett.* **2005**, *87*, 043111−043013.
(33) Li, Q. G.; Penner, R. M. Photoconductive Cadmium Sulfide Hemicylindrical Shell Nanowire Ensembles. *Nano Lett.* **2005**, *5*, 1720−1725.
(34) Lee, J. H.; Lee, P.; Lee, D. J.; Lee, S. S.; Ko, S. H. Cryst. Large-Scale Synthesis and Characterization of Very Long Silver Nanowires via Successive Multistep. *Cryst. Growth Des.* **2012**, *12*, 5598−5605.
(35) Tell, B.; Damen, T. C.; Porto, S. P. S. Raman Effect in Cadmium Sulfide. *Phys. Rev.* **1966**, *144*, 771−774.
(36) Lee, K. Y.; Lim, J. R.; Rho, H.; Choi, Y. J.; Choi, K. J.; Park, J. G. Evolution of Optical Phonons in CdS Nanowires, Nanobelts, and Nanosheets. *Appl. Phys. Lett.* **2007**, *91*, 201901−201903.
(37) Lin, D. D.; Wu, H.; Zhang, W.; Li, H. P.; Pan, W. Enhanced UV Photoresponse from Heterostructured Ag-ZnO Nanowires. *Appl. Phys. Lett.* **2009**, *94*, 172103−172106.
(38) Soci, C.; Zhang, A.; Xiang, B.; Dayeh, S. A.; Aplin, D. P. R.; Park, J.; Bao, X. Y.; Lo, Y. H.; Wang, D. ZnO Nanowire UV Photodetectors with High Internal Gain. *Nano Lett.* **2007**, *7*, 1003−1009.
(39) Prades, J. D.; Hernandez-Ramirez, F.; Jimenez-Diaz, R.; Manzanares, M.; Cirera, T.; Romano-Rodriguez, A.; Morante, J. R.; Andreu, T. The Effects of Electron-hole Separation on the Photoconductivity of Individual Metal Oxide Nanowires. *Nanotechnology* **2008**, *19*, 465501−465507.
(40) Zhai, T. Y.; Fang, X. S.; Liao, M. Y.; Xu, X. J.; Zeng, H. B.; Yoshio, B.; Golberg, D. ZnO Nanowire UV Photodetectors with High Internal Gain. *Sensors* **2009**, *9*, 6504−6529.
(41) Yeh, P. H.; Li, Z.; Wang, Z. L. Aligned Macroscopic Domains of Optoelectronic Nanostructures Prepared via Shear-Flow Assembly of Peptide Hydrogels. *Adv. Mater.* **2009**, *21*, 4975−4978.
(42) Dong, R.; Bi, C.; Dong, Q. F.; Guo, F. W.; Yuan, Y. B.; Fang, Y. J.; Xiao, Z. G.; Huang, J. S. An Ultraviolet-to-NIR Broad Spectral Nanocomposite Photodetector with Gain, Adv. *Adv. Opt. Mater.* **2014**, *2*, 549−554.
(43) Yan, C. Y.; Singh, N. D.; Lee, P. S. Wide-bandgap Zn_2GeO_4 Nanowire Networks as Efficient Ultraviolet Photodetectors with Fast Response and Recovery Time. *Appl. Phys. Lett.* **2010**, *96*, 053108−053111.
(44) Mondal, S. P.; Ray, S. K. Enhanced Broadband Photoresponse of Ge/CdS Nanowire Radial Heterostructures. *Appl. Phys. Lett.* **2009**, *94*, 223119−223121.
(45) Tsutsui, T.; Takada, N.; Saito, S. Control of Spontaneous Emission using Microcavity Structures in Organic Electroluminescent Devices. *Synth. Met.* **1995**, *71*, 2001−2004.
(46) Peng, H. J.; Zhu, X. L.; Sun, J. X.; Xie, Z. L.; Xie, S. A.; Wong, M.; Kwok, H. S. Efficient Organic Light-emitting Diode using Semitransparent Silver as Anode. *Appl. Phys. Lett.* **2005**, *87*, 173505−173507.
(47) Masenelli, B.; Gagnaire, A.; Berthelot, L.; Tardy, J.; Joseph, J. Controlled Spontaneous Emission of a Tri (8-hydroxyquinoline) Aluminum Layer in a Microcavity. *J. Appl. Phys.* **1999**, *85*, 3032−3037.

DOI: 10.1021/acsami.5b06166
ACS Appl. Mater. Interfaces 2015, 7, 22941−22952